# Imaging ocean-basin reverberation via inversion

Nicholas C. Makris

*Naval Research Laboratory, Washington, DC 20375*

A technique for imaging large areas of the ocean floor by inverting reverberation data is presented. Acoustic returns measured on a horizontally towed line array have right–left ambiguity about the array's axis and decreasing cross-range resolution for off-broadside beams and more distant scattering sites. By optimal use of data taken with differing array locations and orientations, right–left ambiguity is eliminated and resolution is maximized. This is accomplished via a global inversion using the array's known resolving properties. The output of the inversion can be optimally resolved reverberation, scattering coefficient, or physical properties of the seafloor, depending upon the formulation. Simulations are presented to show the general superiority of this approach to data averaging.

PACS numbers: 43.30.Gv, 43.30.Pc

## INTRODUCTION

Our goal is to image the ocean basin using acoustic reverberation data. When operating in bottom-limited environments, active sonar systems measure discrete backscatter returns from the seafloor. The nature of these returns depends upon transmission loss as well as the morphology and geo-acoustic properties of the scattering site. By two-way travel-time analysis, the range of particular scattering sites can be deduced for respective returns. Since low-frequency active systems typically measure acoustic returns with a horizontally towed line array, the azimuth of scattering sites can be determined by beamforming. Beamformed line-array data, however, has (a) an inherent right–left ambiguity about the array's axis, (b) decreasing angular resolution for off-broadside beams, and (c) decreasing cross-range resolution for more distant scattering sites. These ambiguities make it difficult to properly locate returns in complex ocean environments where scattering sites are broadly distributed in range and azimuth.[1]

For future reference, we define an "observation" as an active insonification and subsequent towed-array measurement of reverberation at a single location and orientation. (We sometimes use "observation" to refer to the array location in such a measurement.) We define a "reverberation map" as the magnitude of acoustic returns from a single observation charted to the horizontal location of their respective scattering sites. A "scattering strength map" is a reverberation map normalized by source strength, scattering site area, and transmission loss.

Averaging together scattering strength maps has proven to be successful in reducing right–left ambiguity, given a sufficiently diverse observation geometry.[2,3] However, this technique has only been applied to situations where isolated scattering features, such as seamounts or continental margins, disturb sound channels that otherwise have excess depth. It does not work as well for broadly distributed backscattering in complex bottom-limited environments.[4]

Right–left angular ambiguity in ambient noise data has been resolved by an iterative optimization procedure.[5] This can be further applied to resolve angular ambiguity in long-range monostatic and bistatic reverberation data by collapsing towed-array observation locations to a single point and performing angular inversions at independent range steps.[6] However, this approach provides a resolution no finer than the maximum separation between observations. Given spatially distributed observations in complex bottom-limited environments, higher resolution is often necessary for comparisons with seafloor morphology.

We propose a more general imaging method based on a global inversion of spatially distributed observations. In this initial formulation we assume that sound scattered from a particular region is independent of incident and observation angle, in both the horizontal and vertical. This approximation is good for monostatic and bistatic reverberation experiments in the deep ocean, where propagation angles only vary over a narrow vertical width, and the azimuth of distant scatterers remains relatively constant from observation to observation. (It can also be used to make omnidirectional estimates, given a broad distribution of observations, as is shown in a preliminary article.[7])

By simulation, we demonstrate the method for a monostatic observation geometry and operational parameters used in bottom reverberation experiments sponsored by the Office of Naval Research Special Research Program in 1991–1993. We first create a synthetic ocean basin with a scattering coefficient representation, and generate synthetic reverberation maps for the given observation geometry. We then attempt to estimate the true scatter coefficients from the reverberation maps by (a) a linear average, (b) a dB average, and (c) a global inversion. Finally, we test the accuracy of each method by a statistical comparison of the estimated and true scatter coefficients. Since some methods may estimate high scatter coefficients better, we make the above comparison separately for different magnitude regimes.

## I. REVERBERATION MAPS

To compare reverberation measured with differing array positions and orientations, returns from each observa-

## Report Documentation Page

Public reporting burden for the collection of information is estimated to average 1 hour per response, including the time for reviewing instructions, searching existing data sources, gathering and maintaining the data needed, and completing and reviewing the collection of information. Send comments regarding this burden estimate or any other aspect of this collection of information, including suggestions for reducing this burden, to Washington Headquarters Services, Directorate for Information Operations and Reports, 1215 Jefferson Davis Highway, Suite 1204, Arlington VA 22202-4302. Respondents should be aware that notwithstanding any other provision of law, no person shall be subject to a penalty for failing to comply with a collection of information if it does not display a currently valid OMB control number.

| 1. REPORT DATE | 2. REPORT TYPE | 3. DATES COVERED |
|---|---|---|
| **AUG 1993** | | **00-00-1993 to 00-00-1993** |

| 4. TITLE AND SUBTITLE | 5a. CONTRACT NUMBER |
|---|---|
| **Imaging Ocean-basin Reverberation via Inversion** | 5b. GRANT NUMBER |
| | 5c. PROGRAM ELEMENT NUMBER |
| 6. AUTHOR(S) | 5d. PROJECT NUMBER |
| | 5e. TASK NUMBER |
| | 5f. WORK UNIT NUMBER |

| 7. PERFORMING ORGANIZATION NAME(S) AND ADDRESS(ES) | 8. PERFORMING ORGANIZATION REPORT NUMBER |
|---|---|
| **Naval Research Laboratory,4555 Overlook Ave SW,Washington,DC,20375** | |

| 9. SPONSORING/MONITORING AGENCY NAME(S) AND ADDRESS(ES) | 10. SPONSOR/MONITOR'S ACRONYM(S) |
|---|---|
| | 11. SPONSOR/MONITOR'S REPORT NUMBER(S) |

**12. DISTRIBUTION/AVAILABILITY STATEMENT**
**Approved for public release; distribution unlimited**

**13. SUPPLEMENTARY NOTES**

**14. ABSTRACT**

**15. SUBJECT TERMS**

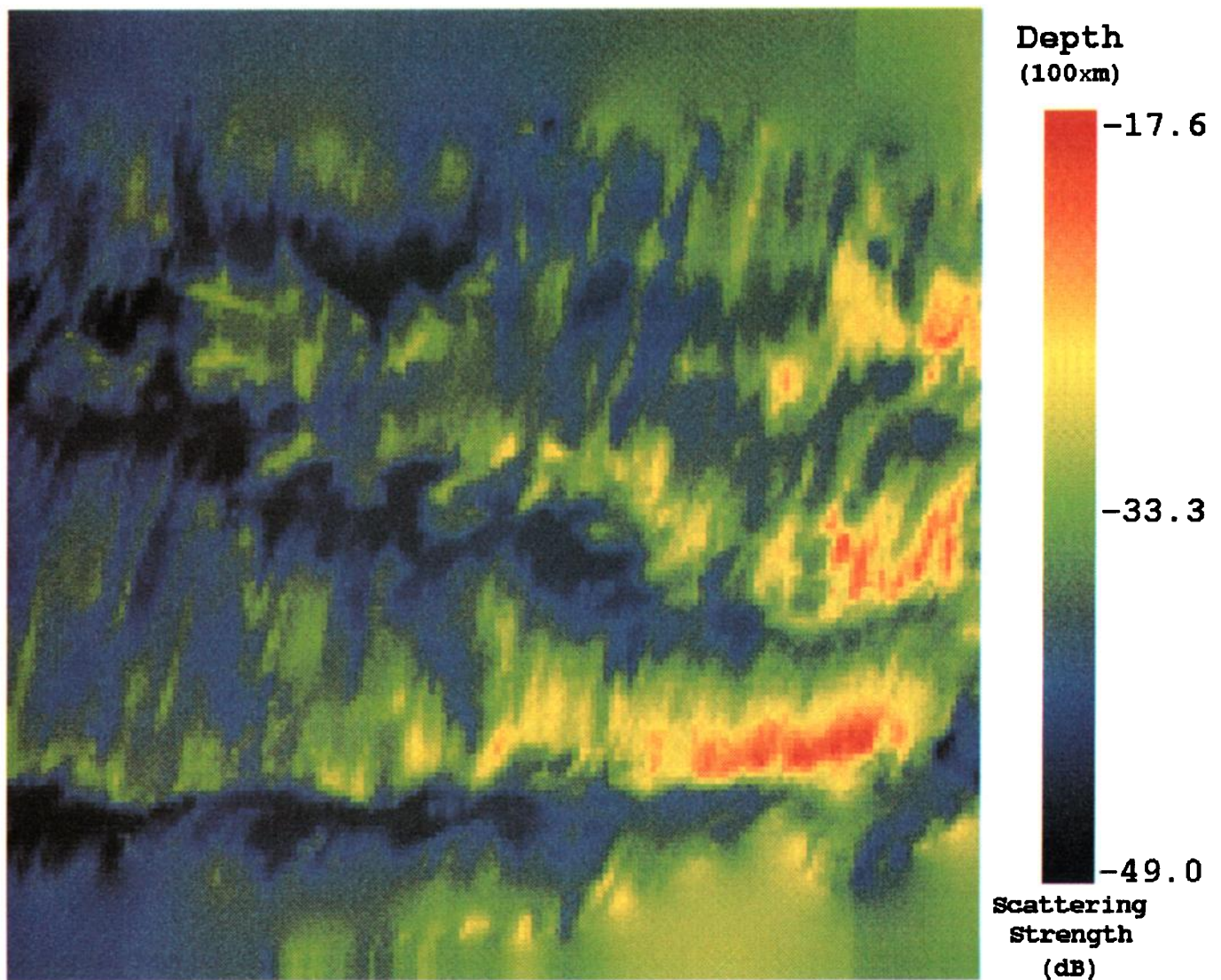| 16. SECURITY CLASSIFICATION OF: | | | 17. LIMITATION OF ABSTRACT | 18. NUMBER OF PAGES | 19a. NAME OF RESPONSIBLE PERSON |
|---|---|---|---|---|---|
| a. REPORT **unclassified** | b. ABSTRACT **unclassified** | c. THIS PAGE **unclassified** | **Same as Report (SAR)** | **11** | |

FIG. 1. The image chosen to represent the ocean basin. Increasing negative values indicate increasing depth as measured from the ocean's upper surface. The data are extracted and subsampled from the SRP Geophysical Survey[9] for a 244×244 km² region. Scattering strength, $\Sigma[m,n]=10\log(\sigma[n,m])$, is chosen to be equal to the numerical value of depth, in hundreds of meters, for respective east versus north grid point coordinates $m=1,2,3,...,N_x$ and $n=1,2,3,...,N_y$, where $N_x=N_y=163$.

tion must be mapped to absolute spatial coordinates. For real data, temporal returns measured on an array of hydrophones can be accurately converted to the range and azimuth of their respective scattering sites. Beamforming yields the necessary azimuthal dependence, but with varying resolution and right–left ambiguity. Travel time can then be linearly converted to range, via mean sound speed, with high accuracy for intermediate ranges larger than a few ocean depths. More complex conversions using depth-dependent slant range or ray travel time are necessary for local returns.[8] For synthetic data, however, it is possible to maintain a spatial representation throughout.

To generate synthetic reverberation maps, we first choose a scattering strength representation of the ocean basin as defined by a single arbitrary image, shown in Fig. 1.[9] We can use a single image because we have assumed that scattering strength is independent of incident and observation angle.

The image is composed of discrete pixels that form a Cartesian array of grid points. We arbitrarily choose scattering strength to be equal to the depth value, in hectometers, of respective pixels in the image. This serves two purposes. It provides scattering strength values that fall within the range typically measured[10] and it describes a scattering region that has variations related to the bathymetry.

We define the scattering coefficient at each grid point by a discrete function $\sigma[m,n]$, which samples the continuous variable $\sigma(x,y)$ according to

$$\sigma[m,n] = \sum_{m=1}^{N_x} \sum_{n=1}^{N_y} \delta(x-m\,\Delta x)\delta(y-n\,\Delta y)\sigma(x,y).$$

$$(1)$$

The scattering coefficient $\sigma[m,n]$ is related to scattering strength via $\Sigma[m,n]=10\log(\sigma[n,m])$ for grid point $m=x/\Delta x$, $n=y/\Delta y$, where $(x,y)$ and $[m,n]$ represent respective

continuous and discrete (east, north) coordinates originating at the southwest corner of the sampled region.

An ideal line array's azimuthal resolution is most commonly described by its 3-dB beamwidth $\beta(\theta)$. For steering angles from broadside, $\theta=\pi/2$, to a transition angle $\theta_t$ near endfire, $\theta=0$,

$$\beta(\theta)=K\frac{\lambda}{L}\frac{1}{\sin\theta},\qquad(2)$$

where $K$ depends on the taper function or window used. We define $\theta_t$ by the value at which the right-hand side of Eq. (2) reaches the endfire beamwidth,[11]

$$\beta(0)=2.16K\sqrt{\lambda/L}.\qquad(3)$$

We approximate $\beta(\theta)=\beta(0)$ for $0\leqslant\theta\leqslant\theta_t$.

The beamwidth of the simulated data is determined by the wavelength $\lambda$, the array aperture $L$, and the taper function. With $\lambda=6.1$ m, $L=160$ m, and $K=1.3$ for a Hamming window, this translates to an azimuthal resolution at broadside of $\beta(\pi/2)=2.8°$. The radial resolution $\Delta r$ is determined by the mean speed of the deep sound channel $c$ and the pulse duration for cw signals $\tau$. For $c=1.5$ km/s and $\tau=2$s, $\Delta r=c\tau/2=1.5$ km. The grid increments $\Delta x$, $\Delta y$ are chosen to be equal to the radial resolution of the simulated data, $\Delta x=\Delta y=\Delta r=1.5$ km.

Reverberation measured a distance $r$ from the array, at an angle $\theta$ from its axis, is comprised of returns weighted over azimuth and integrated within an annulus of width $\Delta r$. The azimuthal weighting is determined by the array's beampattern in the $\theta$ direction. In our inversion and simulations, we ignore the contribution from sidelobes in the beampattern, and approximate the azimuthal weighting by unity within the 3-dB beamwidth $\beta(\theta)$ and zero outside. The integration region is an annular sector of area $r\beta(\theta)\Delta r$ centered about the point $(r,\theta)$. For our purposes, this integration region defines the scattering area for the temporal return mapped to $(r,\theta)$. Contributions from a symmetric annular sector centered at $(r,-\theta)$ are also added to account for the array's right–left ambiguity. This is displayed schematically in Fig. 2.

To generate a synthetic reverberation map for observation $s$, data at grid points within ambiguous annular sectors are summed together incoherently via

$$Q_s[m_0,n_0]=\int_{r_{\min}}^{r_{\max}}\int_{\theta_{\min}}^{\theta_{\max}}\sum_{m=1}^{N_x}\sum_{n=1}^{N_y}\delta(x-m\,\Delta x)$$

$$\times\delta(y-n\,\Delta y)T_s(r,\theta)d\theta\,dr,\qquad(4)$$

$$T_s(r,\theta)=\left[\frac{\sigma(r,\theta)}{2}f_s(r,\theta)+\frac{\sigma(r,-\theta)}{2}f_s(r,-\theta)\right],\qquad(5)$$

where $Q_s[m_0,n_0]$ is the reverberation measured at grid point $m_0=x_0/\Delta x$, $n_0=y_0/\Delta y$. (The selected grid points are also shown in Fig. 2.) Polar and Cartesian coordinates are related by

$$x=r\cos(\theta+\varphi_s)+x_s,\qquad y=r\sin(\theta+\varphi_s)+y_s,\qquad(6)$$

for observation $s$, array axis orientation $\varphi_s$, and array center location $(x_s,y_s)$. The integration limits are
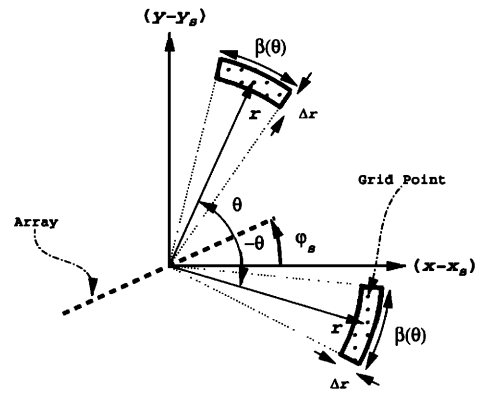


FIG. 2. Synthetic reverberation measured at $(r,\theta)$ from an array positioned at $(x_s,y_s)$. The heavy dotted line indicates the array axis at angle $\varphi_s$ with respect to the Cartesian grid. Symmetric annular sectors about the array axis encompass grid points to be integrated.

$\theta_{\min}=\theta_0-\beta(\theta)/2$, $\theta_{\max}=\theta_0+\beta(\theta)/2$, $r_{\min}=r_0-\Delta r/2$, $r_{\max}=r_0+\Delta r/2$.

The function $f_s(r,\theta)$ consists of two factors $f_s(r,\theta)=g_s(r,\theta)h_s(r,\theta)$. The first factor $g_s(r,\theta)$ incorporates two-way propagation between source and scatterer. For monostatic situations, reciprocity is used on the return trip so that $g_s(r,\theta)=I_s^2(r,\theta)/I_{s0}$ where $-10\log(I_s(r,\theta))$ is the transmission loss at the ocean bottom for horizontal position $(r,\theta)$ and $10\log(I_{s0})$ is the source level. For inversion with actual data, the insonifying field is computed using a range-dependent propagation model such as the wide angle parabolic equation.

However, for this paper we have assumed zero transmission loss and source level, i.e., $g_s(r,\theta)=1$ for all $(r,\theta)$ and $s$. Weighting the data via a complicated propagation model would be lost on our simulations since the weights would simply be removed in the preprocessing stages before the actual inversion. (By similar reasoning, we neglect to convert the data from range to travel time back to range dependence by maintaining a range dependence throughout.)

Due to the right–left ambiguity of the line-array data we expect that $Q_s[m_0,n_0]=Q_s[m_0',n_0']$ when $r_0=r_0'$, $\theta_0=-\theta_0'$ for observation $s$. The correction factor, $h_s(r,\theta)=r\beta(\theta)\Delta r/\eta_s[m,n]$, guarantees that this is so regardless of the grid size, where $m=x/\Delta x$, $n=y/\Delta y$ are related to $(r,\theta)$ by Eqs. (6) for observation $s$. Here the number of grid points per scattering area, or the integration number, is

$$\eta_s[m_0,n_0]=\int_{r_{\min}}^{r_{\max}}\int_{\theta_{\min}}^{\theta_{\max}}\sum_{m=1}^{N_x}\sum_{n=1}^{N_y}\delta(x-m\,\Delta x)$$

$$\times\delta(y-n\,\Delta y)d\theta\,dr,\qquad(7)$$

where the summation limits are as previously defined. This factor is necessary because of approximations made in mapping inherently polar reverberation data onto the Cartesian grid used to digitally define the image. As the grid size decreases with respect to the radial resolution of the array $\Delta r$, the correction factor $h_s(r,\theta)$ approaches unity

and the resolution of the inversion increases. However, it is not advantageous to choose a grid size much smaller than $\Delta r$. As the grid becomes finer than this, the information content remains constant but the inversion time prohibitively increases.

For a given observation, we do not compute reverberation for grid points whose scattering areas extend beyond boundaries corresponding to the edges of the image. We also do not compute reverberation for grid points whose integration numbers exceed a chosen threshold $\eta_{max}$. This insures that redundant information from endfire beams, which is too poor in resolution to be useful, does not slow down the processing. However, thresholding also limits the data available at long range, which eventually limits an inversion's effectiveness at long range.

## II. INVERSION

We initialize our scattering coefficient estimate $\hat{\sigma}[m,n]$ at some value within an allowable range $\sigma_{min} < \hat{\sigma}[m,n] < \sigma_{max}$ for all grid points $m=1,2,3,...,N_x$ and $n=1,2,3,...,N_y$. For each observation $s$, we construct replica data $R_s[m_0,n_0]$ with our estimated scattering coefficient as in Eq. (4), replacing $Q_s[m_0,n_0]$ with $R_s[m_0,n_0]$ and $\sigma[m,n]$ with $\hat{\sigma}[m,n]$. We then compute a least-squares cost function, which sums the difference squared between replica data and true data for each observation and grid point,

$$E(\hat{\sigma}) = \sum_{s=1}^{S} \sum_{m=1}^{N_x} \sum_{n=1}^{N_y} (Q_s[m,n] - R_s[m,n])^2. \qquad (8)$$

Minimization of this cost function with respect to the $\hat{\sigma}[m,n]$ leads to a series of $S$ linear equations for each grid point. This can be seen by expressing the replica data in Eq. (8) in terms of $\hat{\sigma}[m,n]$. For notational economy we convert $[m,n]$ dependence to an index $k=1,2,3,...,N$, where $N=N_xN_y$. We also introduce a sifting function $B_{s,\kappa,k}$ which defines the beamwidth in discrete space $\kappa=1,2,3,...,N$ for observation $s$. It is unity inside the scattering areas about fixed grid point $k$ and its ambiguous image point $k'$, and zero outside these regions:

$$0 = \frac{\partial}{\partial \hat{\sigma}_j} \sum_{s=1}^{S} \sum_{k=1}^{N} \left[ Q_{s,k} - \sum_{\kappa=1}^{N} \hat{\sigma}_\kappa f_{s,\kappa} B_{s,\kappa,k} \right]^2, \qquad (9)$$

where $j=1,2,3,...,N$. This leads to the linear equations

$$Q_{s,j} = \sum_{\kappa=1}^{N} \hat{\sigma}_\kappa f_{s,\kappa} B_{s,\kappa,j} \qquad (10)$$

for each observation $s=1,2,3,...,S$ at each grid point $j=1,2,3,...,N$.

When the number of equations coupled to a particular set of grid points is greater than or equal to the number of grid points coupled, the equations for these grid points are properly constrained. Satisfaction of this criterion for a set of grid points depends upon the observation geometry, local resolution, and integration threshold. Satisfaction of this criterion for all grid points is more stringent than having the overall number of nonidentical equations, which is at least $S(N/2)$, exceed the overall number of unknowns, $N$. [We note that the number of nonidentical equations is

at least $S(N/2)$ due to the Cartesian grid's general lack of symmetry about an arbitrary array axis. If all observations $s$ had array axes symmetric to the grid, i.e., $\varphi_s = (s-1)\pi/4$, the number of nonidentical equations would be limited to $S(N/2)$, due to right–left ambiguity.]

When properly constrained, these equations can be solved for scattering coefficient $\hat{\sigma}_k$ by matrix inversion.[12] Instead, we choose an iterative optimization procedure, because such procedures are extremely efficient in both formulation and solution of problems involving a large number of intricately related parameters. They are ideal for our situation since the images that we need to invert typically contain between $N=10^4$ to $10^6$ pixels and are the result of a highly convoluted process.

Because the problem is linear, we are guaranteed to obtain the correct solution via an iterative random-search for local minima, if the problem is properly constrained. This can also be seen in Eq. (9). The function we are minimizing is parabolic in the parameters to be varied. This insures that the minimum found in the parameter search space is a global minimum. Besides being extremely efficient, this method is also convenient for another reason. Since it is essentially the same as using simulated annealing at zero temperature, it is easily transformed to a simulated annealing algorithm. If there is uncertainty in the observation geometry, i.e., the ship's location and array heading are not precisely known, these parameters can be included in the search. The problem then becomes nonlinear and a simulated annealing approach is necessary to escape local minima in the parameter search space.
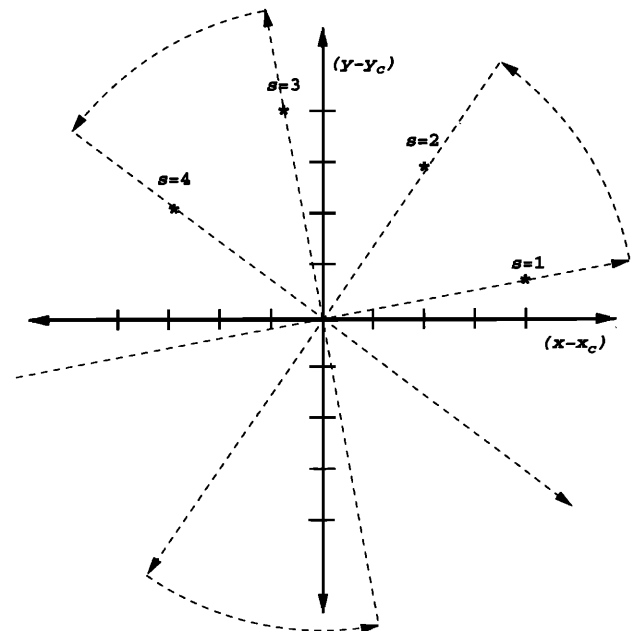


FIG. 3. Synthetic observation geometry with towed-array course indicated by the dotted lines and arrows. The coordinate axis shown is at the center of the region displayed in Fig. 1, i.e., at $m_c = x_c/\Delta r = 81$, $n_c = y_c/\Delta r = 81$, where tick spacing is $\Delta r$. Monostatic observation locations are given by asterisks. Array axis orientations are within $\pm 5°$ of the tracks shown. Specific array positions and orientations $(x_s/\Delta r, y_s/\Delta r, \varphi_s)$ are $(m_c+4, n_c+1, 5°)$, $(m_c+2, n_c+3, 55°)$, $(m_c-1, n_c+4, 114°)$, $(m_c-3, n_c+2, 133°)$, respectively, for the $s=1,2,3,4$ observations.
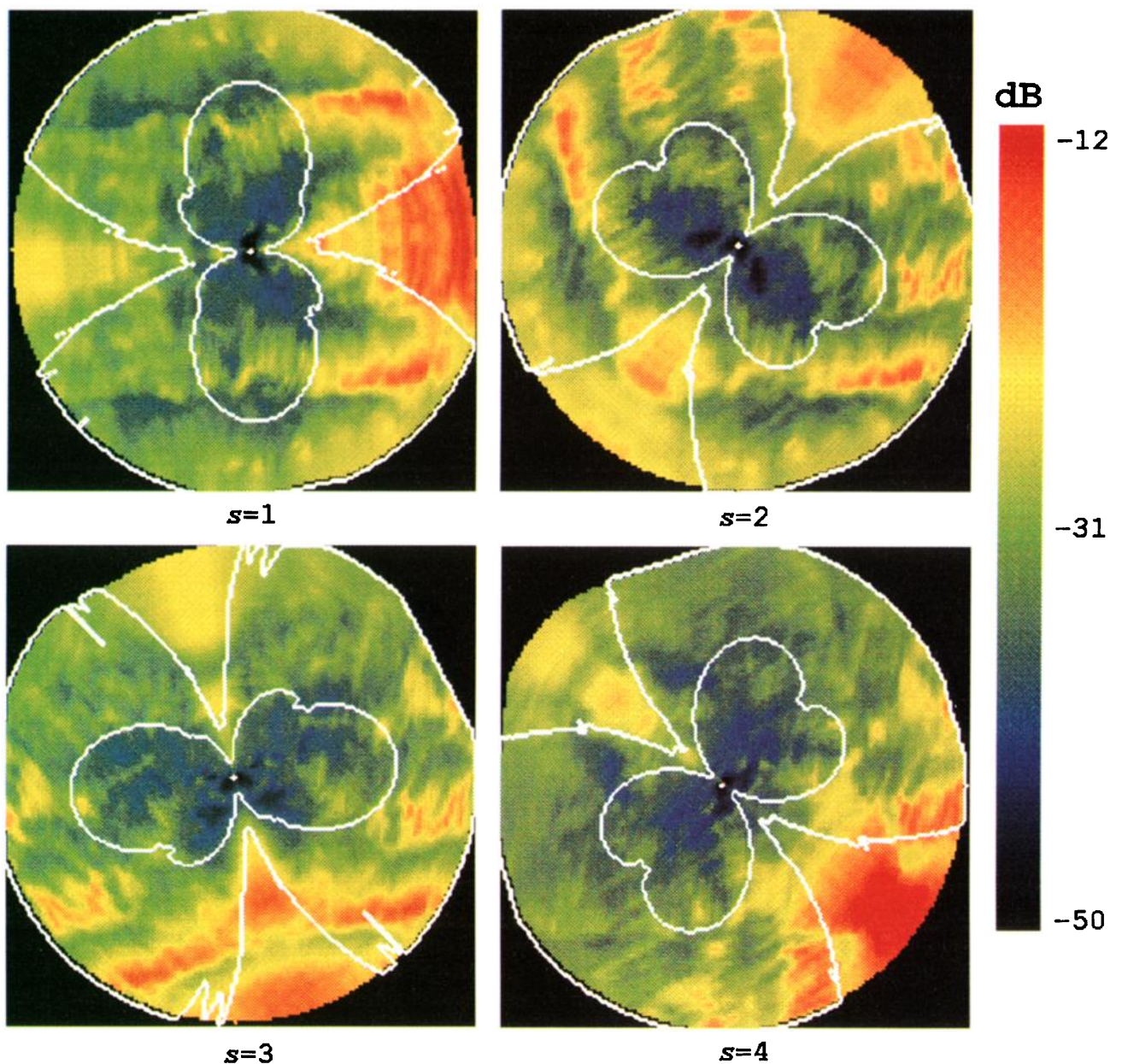
FIG. 4. Synthetic reverberation maps $10 \log(Q_s)$ for the $s=1,2,3,4$ observations. Outside the interior white lines, the resolution is poorer than one grid increment. All data to be used for scatter coefficient estimation are within the exterior white line, i.e., poor resolution data from endfire beams and beyond a threshold range are excluded.

To implement the inversion numerically, we perturb the estimated scattering coefficient $\hat{\sigma}_j$ at a single grid point $j$ by a random multiplicative factor $\epsilon$ such that $\hat{\sigma}'_j = \epsilon \hat{\sigma}_j$, and $\sigma_{min} < \hat{\sigma}'_j < \sigma_{max}$. (Specifically, we choose $\epsilon = 10^{(2\chi-1)^3}$, where $0 \leqslant \chi \leqslant 1$ is a random variable. This is analogous to the method used in Ref. 13 for additive perturbations. When $\epsilon \hat{\sigma}_j < \sigma_{min}$ or $\sigma_{max} < \epsilon \hat{\sigma}_j$ we set $\hat{\sigma}'_j$ equal to $\sigma^2_{min}/\epsilon \hat{\sigma}_j$ or $\sigma^2_{max}/\epsilon \hat{\sigma}_j$, respectively.) The scatter coefficient $\hat{\sigma}_k$ remains the same for all other grid points, i.e., for $k=1,2,3...,N$ but $k \neq j$. We then compute a new cost function $E'$, which is identical to $E$ in all terms except those containing the grid point $j$. When $k=j$, $\hat{\sigma}_j$ is replaced by the perturbed value $\hat{\sigma}'_j$. If the perturbed cost function $E'$ is less than the original cost function $E$ we accept the perturbation, i.e., if $\Delta E = E' - E < 0$. Otherwise we retain the

original value. We continue this process until each grid point has been perturbed, i.e., for $j=1,2,3...,N$. That comprises the first global iteration. We then iterate globally until the cost function reaches a minimum value $E_{min}$ with respect to the $\hat{\sigma}_j$. As discussed in the last paragraph, the resulting $\hat{\sigma}_j$ will be the solution for a properly constrained problem. If the problem is not properly constrained for certain grid points, resolution will be poorer than the grid size and speckling will occur in that portion of the image. Also, ambiguity will be reduced, but may not be eliminated.

In comparing $E'$ to $E$ it is inefficient and prohibitively time consuming to compute each cost function as shown in Eq. (8). Since only a single test grid point has been changed there is no difference between many correspond-
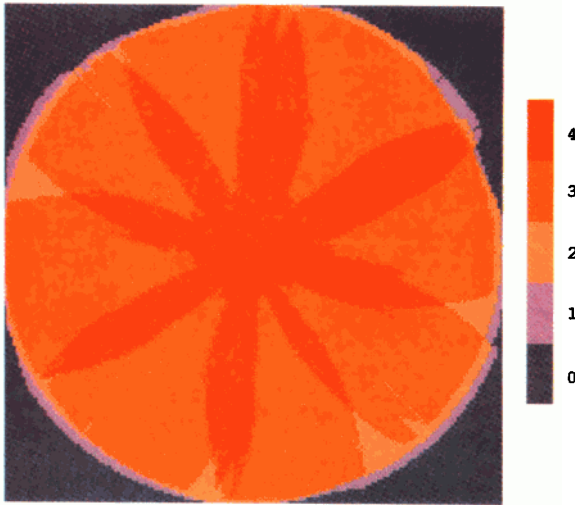
FIG. 5. The number of reverberation maps available per grid point, $\Omega_s$.

ing terms in each summation. Therefore, instead of summing over all $N_x$ and $N_y$ grid points for each perturbation, only a smaller influence region $\Im_s[m-m_0,n-n_0]$ about the test grid point $[m_0,n_0]$ need be considered. In general, the influence region is approximately equal to the integration region of Eq. (7) for a given observation $s$. For observation points related by the array's right–left ambiguity, the influence region must be large enough to account for the lack of perfect reciprocity about the array's axis. As noted earlier, this occurs for array orientations which are not symmetric with respect to the Cartesian grid.

The running time of the algorithm for each global iteration is then proportional to

$$\sum_{s=1}^{S} \sum_{m_0=1}^{N_x} \sum_{n_0=1}^{N_y} \sum_{m=1}^{N_x} \sum_{n=1}^{N_y} \Im_s[m-m_0,n-n_0]. \quad (11)$$

This reduces to a minimum $2N_xN_yS$ when the resolution is equal to the grid size for all observations and grid points, i.e., when
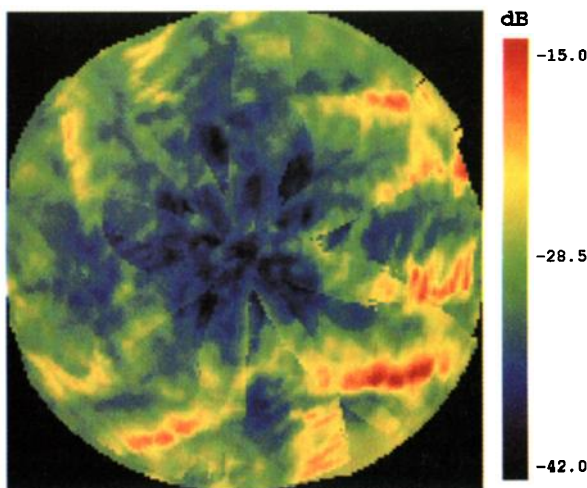


FIG. 6. Scattering strength estimate $\hat{\Sigma}$ from a linear average of reverberation maps.
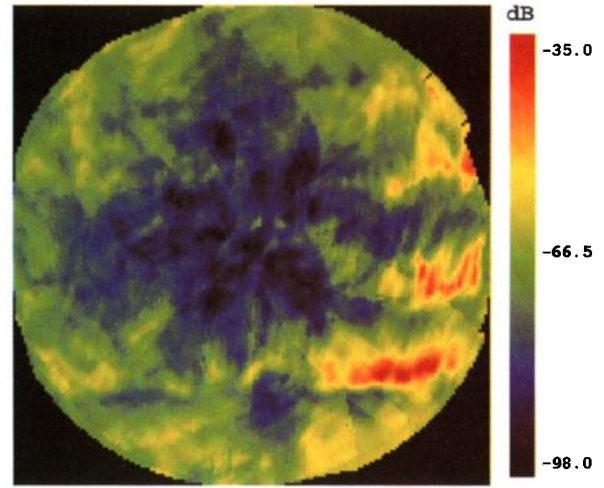


FIG. 7. Scattering strength estimate $\hat{\Sigma}$ from a dB average of reverberation maps.

$$\Im_s[m-m_0,n-n_0] = \delta[m-m_0,n-n_0]$$

$$+\delta[m-m_0'(s),n-n_0'(s)]$$

for all $s$, $n_0$, $m_0$, where $[m_0'(s),n_0'(s)]$ is the ambiguous point for $[n_0,m_0]$ and observation $s$. This minimum run time per global iteration is equal to the overall run time of an average of reverberation maps. As we will show in the next section, however, averaging generally gives an unsatisfactory estimate.

## III. SIMULATION RESULTS

### A. Observation geometry and reverberation maps

Simulations are preformed for the typical monostatic observation geometry sketched in Fig. 3. The ship's course is indicated by dashed lines and arrows. The straight line segments form a star pattern, consisting of four towed-array tracks. Asterisks indicate the location of the observations, where the array axis is roughly parallel to the track. To demonstrate the generality of the method, the tracks are chosen to be asymmetric with respect to the
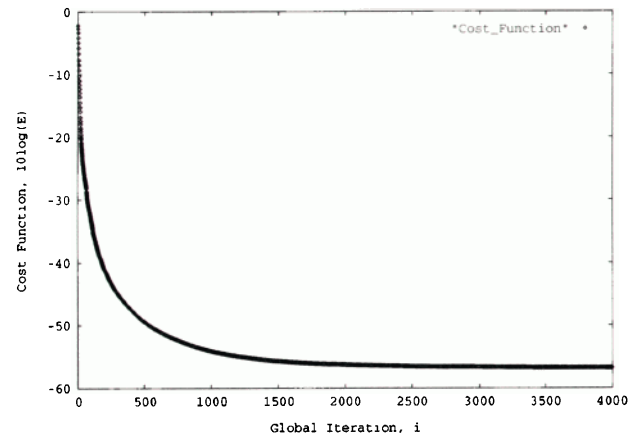


FIG. 8. The cost function $E_i$ versus global iteration $i$ for the scattering coefficient inversion.

TABLE I. Statistical comparison between estimated scatter coefficients $\hat{\sigma}$ and original coefficients $\sigma$. Here, the estimate results from a linear average of reverberation maps. Statistics are computed separately for each of four decades in $\sigma$ and for the same respective grid points in $\hat{\sigma}$. Statistics are only computed for the 21 055 grid points where $1 < \Omega$, see Fig. 9. The percentage of this number for each decade is indicated.

| Linear average | $10^{-5} < \sigma < 10^{-4}$ | $10^{-4} < \sigma < 10^{-3}$ | $10^{-3} < \sigma < 10^{-2}$ | $10^{-2} < \sigma < 10^{-1}$ |
|---|---|---|---|---|
| % | 32.30 | 60.81 | 6.78 | 0.11 |
| $\rho_{\hat{\sigma}\sigma}$ | 0.041 | 0.33 | 0.88 | 0.28 |
| $\langle \hat{\sigma} \rangle / \langle \sigma \rangle$ | 14.19 | 5.01 | 2.58 | 2.11 |

Cartesian grid. Also, to allow for deviations typical in real experiments, the array axes have been randomly perturbed from the track by rotations of within $\pm 5°$.

A synthetic reverberation map $10 \log(Q_s[m,n])$, where $m = 1,2,3,...,N_x$, $n = 1,2,3,...,N_y$, for each observation, $s = 1,2,3,...,S$, is shown in Fig. 4. Note the decrease in resolution for beams approaching endfire and for distant scattering areas, as well as the right–left ambiguity about the array's axis. The interior white contour encompasses data with spatial resolution equal to the grid increment, i.e., the scattering areas contain a single grid point so that $\eta = 1$. Outside this contour, resolution is poorer, i.e., the scattering areas contain multiple grid points and $1 < \eta$. Due to discretization, these contours vary with observation location and ambiguous lobes are not symmetric with respect to the array axes. The exterior white contours encompass data to be used in subsequent scatter coefficient estimation. These data are within the selected $\eta_{max} = 10$ integration number threshold and are also limited by a maximum range from each observation location $(x_s, y_s)$ such that $R_{max} = 83 \Delta r = 124.5$ km, which spans about two deep ocean convergence zones. Data outside these borders are considered to have resolution too poor to be useful.

Due to thresholding, the mapping $Q_s[m_0, n_0]$ may not exist at grid point $[m_0, n_0]$ for observation $s$. To quantify this for the given observation geometry, the number of mappings per grid point $\Omega[m,n]$ is shown in Fig. 5.

## B. Estimate via linear average

We first show the scattering strength estimate resulting from a linear average of reverberation maps. We add all mappings $Q_s[m_0, n_0]$ of grid point $[m_0, n_0]$ and divide by the number of mappings, $0 \leq \Omega[m_0, n_0] \leq S$, for that grid point. The resulting scattering coefficient estimates $\hat{\sigma}[m,n]$ are converted to scattering strengths via $\hat{\Sigma}[m,n] = 10 \log(\hat{\sigma}[m,n])$, for $m = 1,2,3,...,N_x$, and $n = 1,2,3,...,N_y$. The resulting image, in Fig. 6, bears a poor resemblance to the actual scattering strength image in Fig. 1. In general, the magnitude and shape of estimated scattering features

are significantly different from the actual ones. Artificial features of high scattering strength also appear due to imperfect removal of right–left ambiguity.

To quantify these differences, and so test the accuracy of the estimate, we compute the ratio of the means and normalized covariance for the original and estimated scattering coefficients. We compute these statistics independently for sets of grid points corresponding to 10-dB scattering strength bins in the original image, and only examine grid points where the number of mappings $\Omega[m,n] > 1$. The results are in Table I, where we use

$$\rho_{\hat{\sigma}\sigma} = \frac{\langle (\hat{\sigma} - \langle \hat{\sigma} \rangle)(\sigma - \langle \sigma \rangle) \rangle}{\sqrt{\langle (\hat{\sigma} - \langle \hat{\sigma} \rangle)^2 \rangle \langle (\sigma - \langle \sigma \rangle)^2 \rangle}} \quad (12)$$

to define the normalized covariance so that $0 \leq \rho_{\hat{\sigma}\sigma} \leq 1$. We see that the correlation is only high for a small portion of the region imaged, where high amplitude scatter coefficients are found. The mean value is estimated best for these high amplitude coefficients, but is still only within a factor of 3 of the true coefficients.

## C. Estimate via dB average

We next compute the scattering strength estimate resulting from a dB average of reverberation maps, i.e., we add all mappings $10 \log(Q_s[m,n])$ and again divide by $\Omega[m,n]$. The resulting image, Fig. 7, has better right–left ambiguity reduction than the linear estimate, but still resembles the original image only poorly. The comparison is again made quantitative by computing cross statistics, as indicated in Table II. While correlations have generally increased, they are still low, except for a small fraction of the region corresponding to the high amplitude scatterers. However, the mean estimate is orders of magnitude worse than in the linear average.

## D. Estimate via global inversion

The global inversion method provides a solution with minimum cost function $E_{min} \approx E_{4000} = E_0(2.77 \times 10^{-5})$, where the corresponding global iteration number $i$ appears

TABLE II. Statistical comparison between dB average estimate and original scatter coefficients. See Table I caption for further details.

| dB Average | $10^{-5} < \sigma < 10^{-4}$ | $10^{-4} < \sigma < 10^{-3}$ | $10^{-3} < \sigma < 10^{-2}$ | $10^{-2} < \sigma < 10^{-1}$ |
|---|---|---|---|---|
| % | 32.30 | 60.81 | 6.78 | 0.11 |
| $\rho_{\hat{\sigma}\sigma}$ | 0.059 | 0.53 | 0.81 | 0.26 |
| $\langle \hat{\sigma} \rangle / \langle \sigma \rangle$ | $9.25 \times 10^{-4}$ | $8.34 \times 10^{-4}$ | $5.27 \times 10^{-3}$ | $1.68 \times 10^{-2}$ |

as a subscript. Here, the cost function is given in terms of the initial "energy" $E_0$, which is obtained by setting the replica data $R_s[m,n]$ to zero in Eq. (8). The cost function is plotted as a function of global iteration in Fig. 8.

The scattering strength estimate for the global inversion is shown in Fig. 9, where the white contour contains grid points where $1 < \Omega$. As expected from the dramatic decrease in the cost function, the global inversion image is nearly identical to the true image in Fig. 1. The right–left ambiguity of the data has been removed and the ocean basin is resolved to the grid increment in areas where reverberation mappings of such high resolution do not exist. This is confirmed quantitatively in Table III, where near perfect correlation is found between the inversion estimate and the actual scatter coefficients. The mean values are identical.

We note that both high and low values are found with equal precision in the inversion. However, low values are more statistically sensitive to the successive approximations since they are given less weight in the cost function, when considered individually. As a result, more iterations may be necessary to reduce the variance of the estimate for lower values. This is shown in Fig. 10 and Table IV, where the scatter coefficient estimate and cross statistics are provided for intermediate iterations. For inversions with real data, this means that if the cost function reaches an early minimum, i.e., it is reduced by less than an order of magnitude, a statistical analysis is necessary to interpret the estimate. (One possible way of reducing the number of iterations necessary to reach a minimum is to make the perturbation decrease in magnitude as a function of theit-eration. This has not been done for the present analysis, but we have performed some simulations along this line which show that the idea is promising.)

Even if there are no reverberation mappings for a particular grid point, due to thresholding or nearness to a border, the scattering coefficient can still be determined by global inversion if the scattering areas of adjacent mapped points leak onto the unmapped point enough times. Comparing the number of mappings per grid point, Fig. 5, with the inversion estimate, in Fig. 9, we note that this is the case for a variety of grid points at the image periphery. It
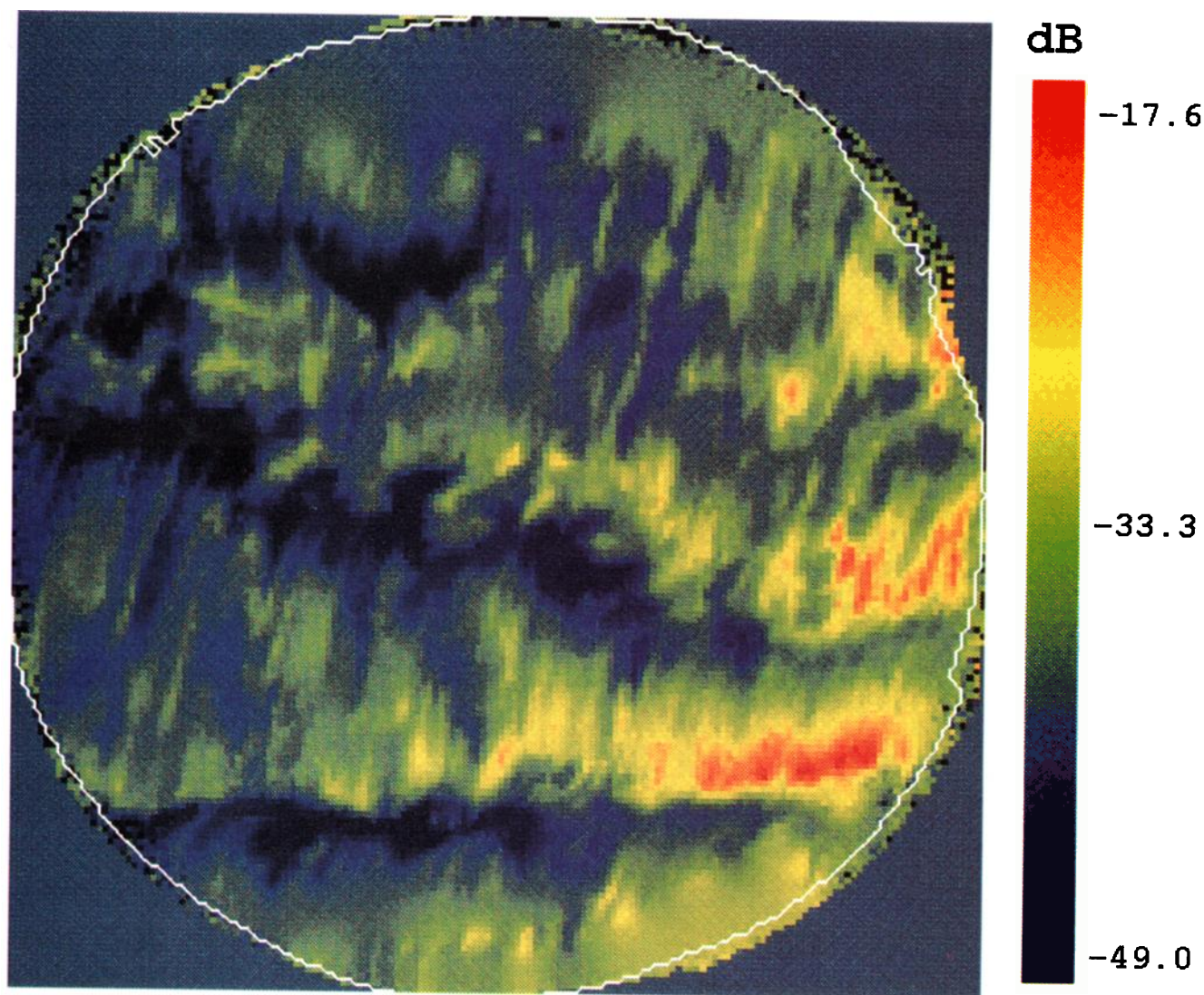


FIG. 9. Scattering strength estimate $\hat{\Sigma}$ from a global inversion of reverberation maps, with corresponding global minimum $E_{min} \approx E_{4000} = E_0(2.77 \times 10^{-5})$. The white line encompasses grid points where $1 < \Omega$.

TABLE III. Statistical comparison between global inversion estimate and original scatter coefficients. Estimate has corresponding cost function approximately at global minimum, $E_{min} = E_{4000} = E_0(2.77 \times 10^{-5})$. See Table I caption for further details. (For grid points where $3 < \Omega, \rho_{\hat{\sigma}\sigma} = 1.0$ when $10^{-5} \leqslant \sigma < 10^{-4}$.)

| Global inversion | $10^{-5} \leqslant \sigma < 10^{-4}$ | $10^{-4} \leqslant \sigma < 10^{-3}$ | $10^{-3} \leqslant \sigma < 10^{-2}$ | $10^{-2} \leqslant \sigma < 10^{-1}$ |
|---|---|---|---|---|
| % | 32.30 | 60.81 | 6.78 | 0.11 |
| $\rho_{\hat{\sigma}\sigma}$ | 0.93 | 1.00 | 1.00 | 1.00 |
| $\langle \hat{\sigma} \rangle / \langle \sigma \rangle$ | 1.00 | 1.00 | 1.00 | 1.00 |

is also clear that the leakage is insufficient to properly estimate scattering strength for some other peripheral grid points.

## IV. DISCUSSION

We have developed a method for imaging the ocean basin via a simultaneous inversion of multiple reverberation measurements made at differing spatial locations. By optimal use of the data, this method removes the right–left ambiguity associated with line-array data and produces as fine a resolution as possible. The method has been tested with a typical monostatic observation geometry where it has proven to be far superior to data averaging for simulations involving reverberation from scattering sites



$E_{12} = E_0 \times 10^{-1}$

$E_{29} = E_0 \times 10^{-2}$

$E_{202} = E_0 \times 10^{-3}$

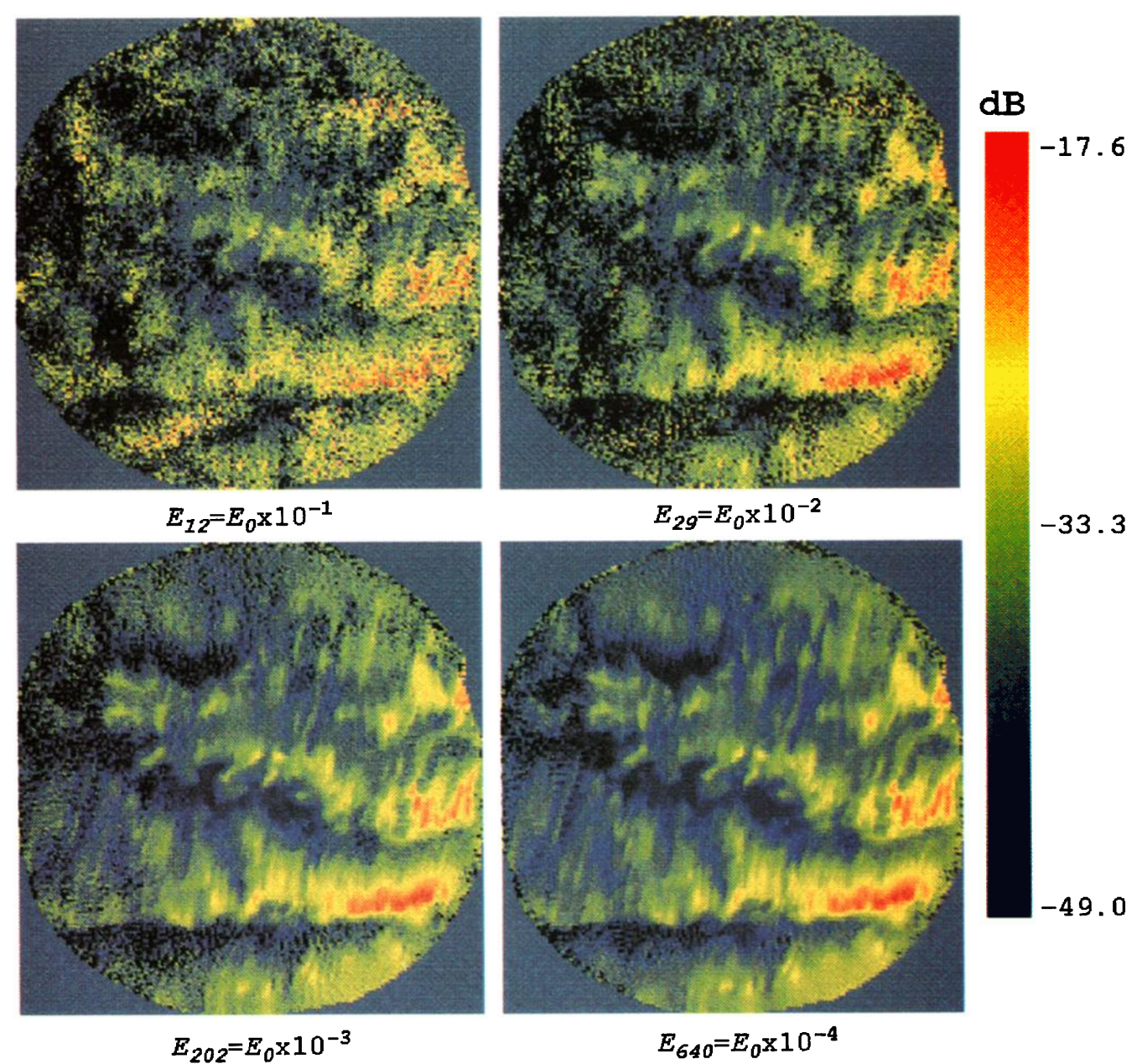$E_{640} = E_0 \times 10^{-4}$

dB

−17.6

−33.3

−49.0

FIG. 10. Intermediate scattering strength estimates $\hat{\Sigma}$ from a global inversion of reverberation maps for indicated iterations.

TABLE IV. Statistical comparison between four intermediate global inversion estimates and original scatter coefficients. See Table I caption for further details.

| Intermediate iterations | $10^{-5}<\sigma<10^{-4}$ | $10^{-4}<\sigma<10^{-3}$ | $10^{-3}<\sigma<10^{-2}$ | $10^{-2}<\sigma<10^{-1}$ |
|---|---|---|---|---|
| % | 32.30 | 60.81 | 6.78 | 0.11 |
| | | $(E_{12}=E_0\times10^{-1})$ | | |
| $\rho_{\hat\sigma\sigma}$ | 0.030 | 0.33 | 0.44 | 0.17 |
| $\langle\hat\sigma\rangle/\langle\sigma\rangle$ | 2.09 | 1.15 | 0.80 | 0.49 |
| | | $(E_{29}=E_0\times10^{-2})$ | | |
| $\rho_{\hat\sigma\sigma}$ | 0.12 | 0.65 | 0.80 | 0.39 |
| $\langle\hat\sigma\rangle/\langle\sigma\rangle$ | 1.26 | 1.01 | 0.98 | 0.86 |
| | | $(E_{202}=E_0\times10^{-3})$ | | |
| $\rho_{\hat\sigma\sigma}$ | 0.47 | 0.95 | 1.00 | 0.97 |
| $\langle\hat\sigma\rangle/\langle\sigma\rangle$ | 1.02 | 1.00 | 1.00 | 0.99 |
| | | $(E_{640}=E_0\times10^{-4})$ | | |
| $\rho_{\hat\sigma\sigma}$ | 0.78 | 0.99 | 1.00 | 1.00 |
| $\langle\hat\sigma\rangle/\langle\sigma\rangle$ | 1.00 | 1.00 | 1.00 | 1.00 |

broadly distributed in space and scattering strength magnitude. In situations where only isolated scatterers of high amplitude are present, and these do not interfere in ambiguous beams, data averaging may suffice. However, this situation is the exception for most ocean environments. A more robust method, such as the inversion presented, is generally necessary.

While the method is currently applicable to many long- and short-range monostatic and bistatic experiment geometries, it cannot be applied arbitrarily. For example, a series of separate inversions is necessary to determine the angular dependence of bottom reverberation. In each inversion, the separation between observations must be small enough to maintain a similar orientation to the region being imaged. This insures that the differences between observation angle are small with respect to variations in the angular dependence being measured.

Alternatively, it is possible to reformulate the inversion to search directly for regional angular dependence via a single global inversion. However, this approach runs into difficulties for ocean environments dominated by negative excess depth and rugged bathymetry due to extreme variations in transmission loss that can make spatially divergent observations independent of each other.[4] For example, regions of extremely high transmission loss, or shadow zones, may exist where no useful scattering information can be extracted. Under these circumstances scaling by transmission loss is not appropriate and redundant information vital to ambiguity resolution may be lost. A simple way to circumvent this problem is to invert observations sufficiently close that their respective transmission loss functions are approximately the same and to exclude data when transmission loss exceeds a threshold maximum. Optimally resolved linear reverberation would then be the output of the inversion rather than scattering coefficient.

On the other hand, variations in transmission loss along ambiguous radials can be used more advantageously than has been suggested. These variations often provide additional environmental symmetry breaking information

that can be exploited to help resolve right–left ambiguity for a single observation, as is demonstrated in an upcoming article.[4] The present inverse method can be readily modified to exploit these situations,[8] and provide a means of directly estimating the regional angular dependence of scattering via a single global inversion of spatially divergent observations.

No attempt has been made to account for statistical variations in reverberation that may arise at differing observation locations. While such stochastic phenomenon are possible in real data, they are not relevant to this initial formulation. Our goal is principally to show that there are ways to make optimal use of towed-array data that are independent of the often stochastic nature of the reverberation. And, even if high variance exists, an ensemble of observations with redundant geometry may be used in the present formulation to make the problem statistically overdetermined and so reduce the variance by the number of redundant observations. Alternatively, stochastics can be incorporated by searching for probability distributions to parametrize seafloor scattering rather than mean scattering coefficient values. If the reverberation is inherently deterministic, i.e., the scattering surfaces are much larger than a wavelength and approximately planar, or the variance is sufficiently low, only observations sufficient to remove ambiguity and obtain the desired resolution would be required, as in the simulations presented.

Finally, we contend that it is possible to determine the optimal set of observations needed to image the ocean bottom with methods related to those presented. That is, assuming some or no knowledge of regional bottom scattering, and given constraints upon our resolution, ship maneuverability, time, site locations, etc., we could invert for the optimal course of the research vessel. This has been referred to as the "traveling acoustician problem." [14] Qualitatively, the problem is related to the much simpler problem of refining the array's navigation by including it as a free parameter in the reverberation inversion. Both prob-

lems are nonlinear, and are most efficiently solved with a technique like simulated annealing.

## ACKNOWLEDGMENTS

[1] J. M. Berkson, N. C. Makris, R. Menis, T. L. Krout, and G. L. Gibian, "Long-range measurements of sea-floor reverberation in the Mid-Atlantic Ridge area," in *Ocean Reverberation*, edited by D. Ellis, J. Preston, and H. Urban (Kluwer, Dordrecht, 1993).

[2] F. T. Erskine, G. M. Bernstein, S. M. Brylow, W. T. Newbold, R. C. Gauss, E. R. Franchi, and B. B. Adams, "Bathymetric Hazard Survey Test (BHST Report No. 3), Scientific Results and FY 1982–1984 Processing," NRL Report 9048 (1987).

[3] J. R. Preston, T. Akal, and J. M. Berkson, "Analysis of backscattering data in the Tyrrhenian Sea," J. Acoust. Soc. Am. **87**, 119–134 (1990).

[4] N. C. Makris and J. M. Berkson, "Long-Range Backscatter from the Mid-Atlantic Ridge," submitted to J. Acoust. Soc. Am.

[5] R. A. Wagstaff, "Iterative technique for ambient-noise horizontal-directionality estimation from towed line-array data," J. Acoust. Soc. Am. **63**, 863–869 (1978).

[6] R. A. Wagstaff, M. R. Bradley, and M. A. Herbert, "The Reverberation Array Heading Surface," in *Ocean Reverberation*, edited by D. Ellis, J. Preston, and H. Urban (Kluwer, Dordrecht, 1993).

[7] N. C. Makris, J. M. Berkson, W. A. Kuperman, and J. S. Perkins, "Ocean-Basin Scale Inversion of Reverberation Data," in *Ocean Reverberation*, edited by D. Ellis, J. Preston, and H. Urban (Kluwer, Dordrecht, 1993).

[8] A paper on mapping, inverting, and projecting high-resolution direct-path reverberation onto bathymetry for Mid-Atlantic Ridge data is in preparation for submission to J. Acoust. Soc. Am.

[9] The bathymetry shown is subsampled from the SRP Geophysical Survey of 1992 which had Principal Investigator Brian E. Tucholke and Co-Principal Investigators Martin C. Kleinrock and Jian Lin, all from the Woods Hole Oceanographic Institution.

[10] P. M. Ogden and F. T. Erskine, "Low-frequency Surface and Bottom Scattering Strengths Measured Using SUS Charges," in *Ocean Reverberation*, edited by D. Ellis, J. Preston, and H. Urban (Kluwer, Dordrecht, 1993).

[11] B. D. Steinberg, *Principles of Aperture and Array System Design* (Wiley, New York, 1976).

[12] G. Strang, *Linear Algebra and Its Applications* (Academic, New York, 1980).

[13] W. A. Kuperman, M. D. Collins, J. S. Perkins, and N. R. Davis, "Optimal Time Domain Beamforming with Simulated Annealing including application of *a priori* information," J. Acoust. Soc. Am. **88**, 1802–1810 (1990).

[14] Private communication with W. A. Kuperman. A paper on the "traveling acoustician problem" is in preparation.